SUPPORTING INFORMATION

Harnessing Scanning Probe Lithography for Integrated Photonics with Anisotropic Materials

Received 00th January 20xx,
Accepted 00th January 20xx

DOI: 10.1039/x0xx00000x

Alexey Kuznetsov[a,b], Bogdan R. Borodin[c], Maria A. Anikina[a,b], Konstantin V. Kravtsov[a], Fedor M. Maksimov[a,d], Artem N. Abramov[e], Adilet N. Toksumakov[f], Eseniya S. Zavyalova[a,e], Valeriy M. Kondratev[a,b], Aleksandra V. Nikolaeva[a,b], Dmitriy Grudinin[f], Aleksandr S. Slavich[f], Vasily Kravtsov[e], Alexander I. Chernov[a,d], Ivan A. Kruglov[a,f], Aleksey V. Arsenin[a,f], Prokhor Alekseev[c], Valentyn S. Volkov[f] and Alexey D. Bolshakov[a,b]*

Numerical modelling

Geometries of the simulated waveguide cross-sections are presented in Figure S1a. For eigenmodal analysis and transmittance simulations, a non-uniform rectangular grid was used with a maximum spatial step of 2 nm (Figure S1b,c). The boundary conditions had to absorb all incident power; thus, a perfectly matched layer was set at all boundaries. Transmittance spectra were calculated in the range of 400–800 nm by injecting the fundamental mode into the waveguide and registering the power flux through the rectangular cross-section (Port "Out"), which was located at a distance of 5 μm from the source (Port "In") as shown in Figure S1c. Calculations were carried out at a single wavelength with a wavelength step of 2 nm to avoid issues with optical constants data approximation. At each step, the field profile of the mode to be injected was recalculated. Port "Out" dimensions matched the waveguide cross-section geometry.

Propagation losses for the fundamental mode of square, TE, and TM strip waveguide cross-section geometries are represented in Figure S2. Square and TE waveguides (Figure S2a,b) demonstrate similar curve behavior: high losses in the intrinsic absorption range (<500 nm) and gradual growth in the longer wavelength range due to mode field delocalization. Losses in the TM waveguide are lower by an order of magnitude due to the zero imaginary part of the out-of-plane refractive index component. Despite this, an increase in propagation losses also occurs starting from 580 nm due to mode leakage.

[a.] *Moscow Center for Advanced Studies, Kulakova str. 20, Moscow, 123592, Russia*
[b.] *Alferov University, Khlopina str. 8/3, Saint-Petersburg, 194021, Russia*
[c.] *Ioffe Institute, Polytekhnicheskaya str., 26, Saint-Petersburg, 194021, Russia*
[d.] *Russian Quantum Center, Novaya str.100, Skolkovo Village, Moscow region, 143026, Russia*
[e.] *ITMO University, Kronverksky Pr. 9, Saint-Petersburg, 197101, Russia*
[f.] *Emerging Technologies Research Center, XPANCEO, Internet City, Emmay Tower, Dubai, United Arab Emirates*
Supplementary Information available: [details of any supplementary information available should be included here]. See DOI: 10.1039/x0xx00000x

Supporting Information

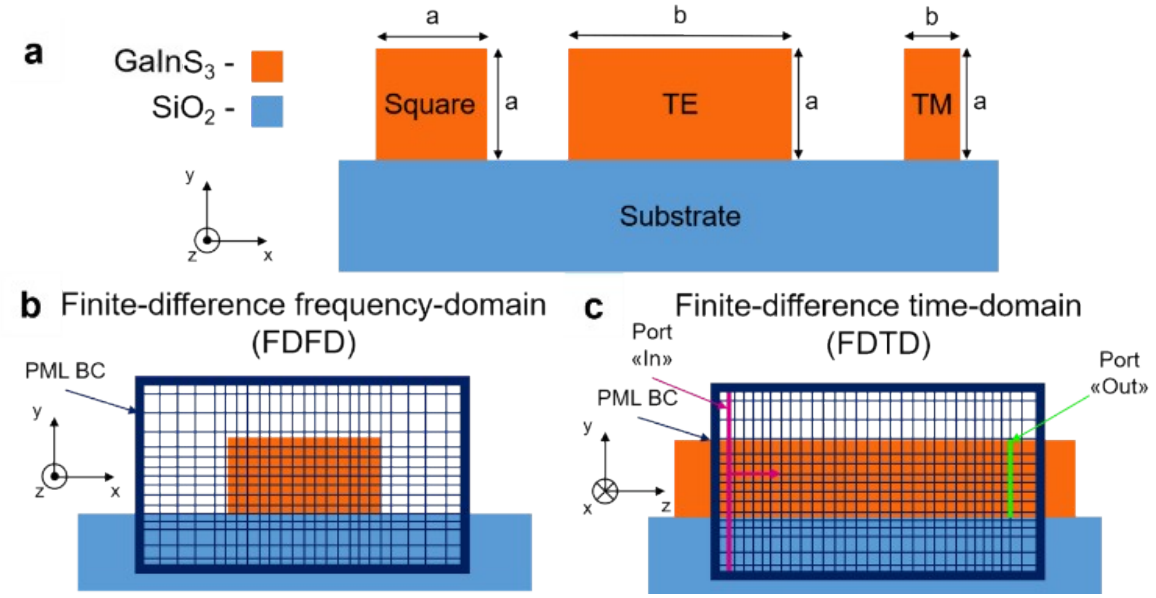

Figure S1. a) Cross-section schematic for the square, TE and TM waveguides with non-uniform spatial grid and for b) FDFD and c) FDTD simulations.

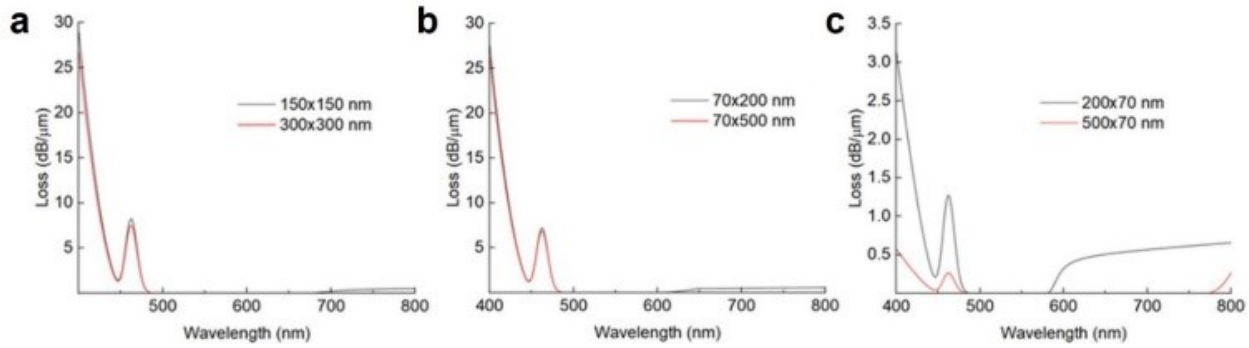

Figure S2. Calculated spectra of the fundamental mode propagation losses for a) square, b), c) TE and TM waveguides of different geometry.

Raman spectroscopy

Figure S3 demonstrates a typical Raman spectrum of the studied $GaInS_3$ flake on a Si/SiO_x substrate, which reveals inherent phonon modes and agrees well with reference [1]. Measurements were performed at room temperature using a Horiba LabRAM HR 800 spectrometer equipped with a 100× (NA = 0.9) objective and a CW solid-state laser with a wavelength of 532 nm (3 mW).

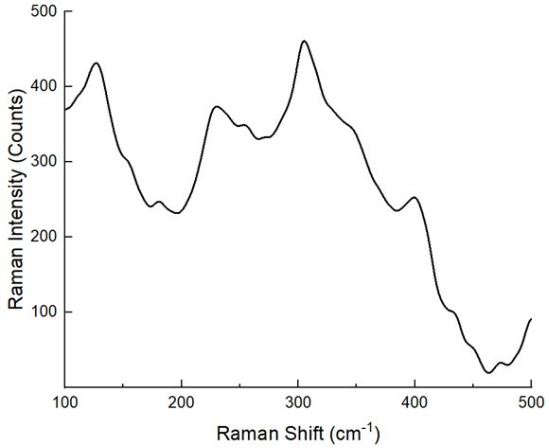

Figure S3. Typical Raman spectrum of the $GaInS_3$ flakes.

$GaInS_3$ mechanical properties modelling

The ability of the interatomic potentials MatterSim and PET-MAD to accurately describe bond breaking and predict ultimate tensile and fracture strengths is an assumption based on their generally high accuracy for other mechanical properties.[2,3] Our calculated stress-strain curves confirm the presence of significant mechanical anisotropy. This anisotropy, combined with differences in the failure mechanisms along distinct crystallographic directions, may be the key reason behind the observed anisotropic nanoscale cutting behavior using an AFM tip. Specifically, we infer that the ultimate tensile and fracture strengths of $GaInS_3$ under strain along the armchair direction should be higher than those along the zigzag direction. This conclusion is supported by analogy with other materials possessing hexagonal structures, for which DFT calculations are available: in such systems, tensile strain along the armchair direction consistently results in higher ultimate and fracture strengths and the corresponding stress-strain curve lies above that for the zigzag direction. In Figure S4, we present our results obtained using the interatomic potentials, alongside DFT data from previous studies for the following materials: silicene and germanene,[4] 2H-MoS_2 and 2H-WS_2,[5] and 2H-$MoTe_2$.[6] Notably, the stress-strain behavior predicted by the potentials agrees well with DFT results across all considered materials, except for one case — 2H-$MoTe_2$ using the PET-MAD potential.

Therefore, using generalized interatomic potentials to compute stress-strain curves along the armchair and zigzag directions leads to the conclusion that $GaInS_3$ is more difficult to cut with an AFM tip along the zigzag direction, while cutting along the armchair direction is significantly easier (see Figure S5).

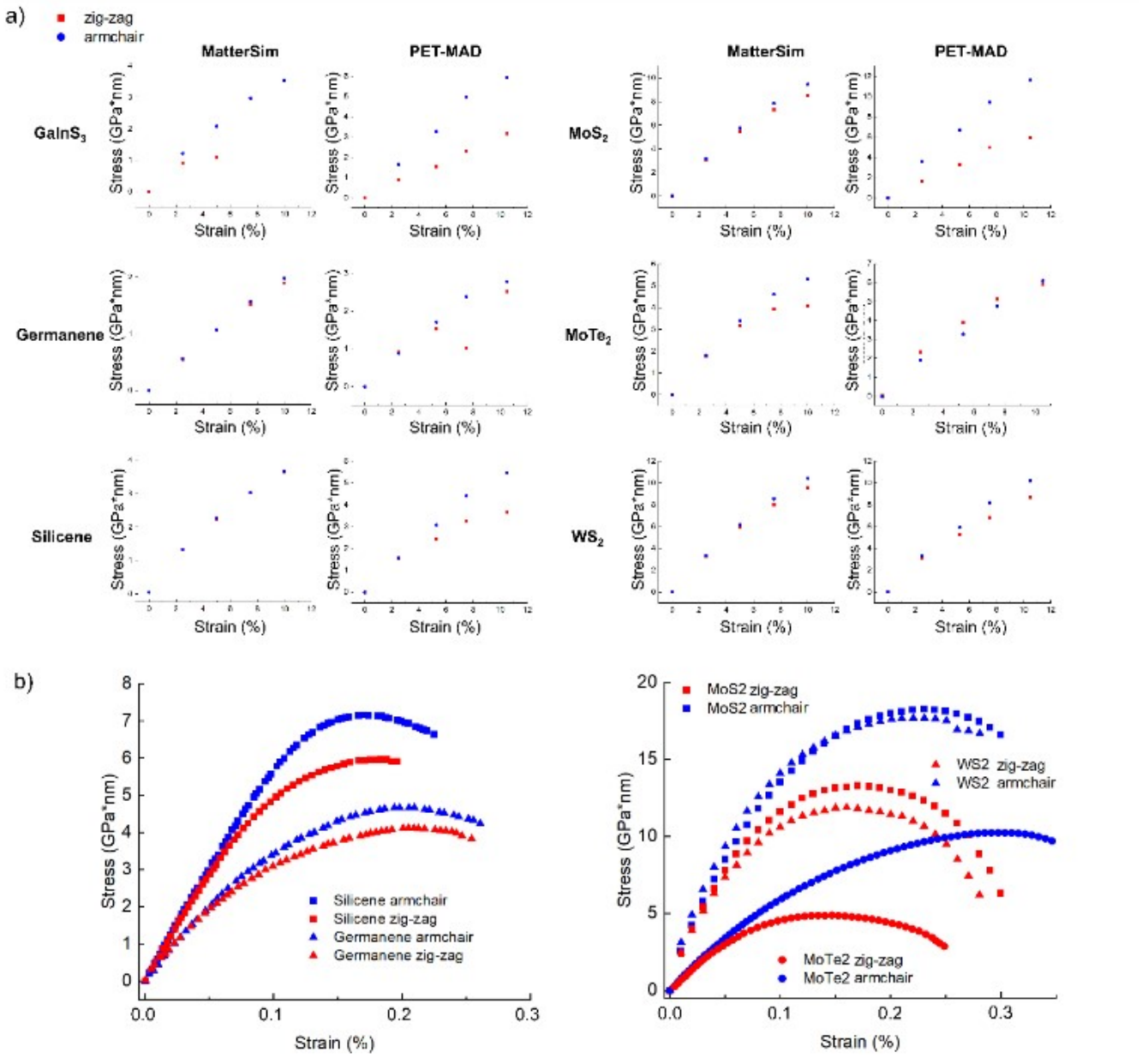

Figure S4. a) Stress-strain curves for different 2D materials with hexagonal lattice symmetry calculated using universal machine learning interatomic potentials MatterSim and PET-MAD and b) same curves adapted from [4-6] for comparison calculated using DFT

.

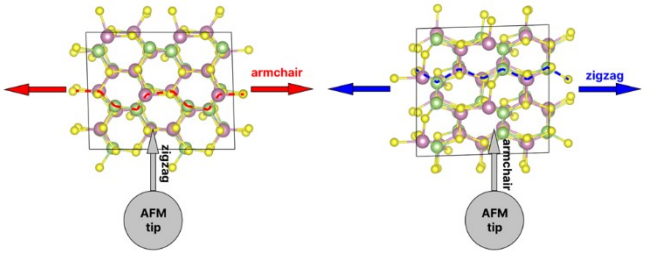

Figure S5. Top view of deformation processes of single-layer $GaInS_3$ (top). Strains along armchair (top left) and zigzag (top right) directions correspond to movement of AFM tip along zigzag and armchair directions respectively.

Optical setup

A schematic of the optical setup for transmittance measurements is illustrated in Figure S6. To measure the transmittance of the fabricated waveguides, it was necessary to focus the SC laser beam into a small spot (~1–3 µm) and distinguish excitation and collection areas within the objective's (100×, NA = 0.9, Mitutoyo Apo HR) field of view. To do so, we used a beam expander to provide better excitation focusing and utilized a spectrometer (Optosky ATP5020) whose fibre (core diameter – 50 µm) was connected to a kinetic mount with an iris diaphragm placed in the back focal plane of the objective. Thus, the collection area coincided with a projection of the fibre core in the image plane. The excitation was focused on one waveguide end, and the collection spot was moved by the kinetic fibre mount to the other end. The collection area size was reduced to ~1 – 2 µm using the iris diaphragm.

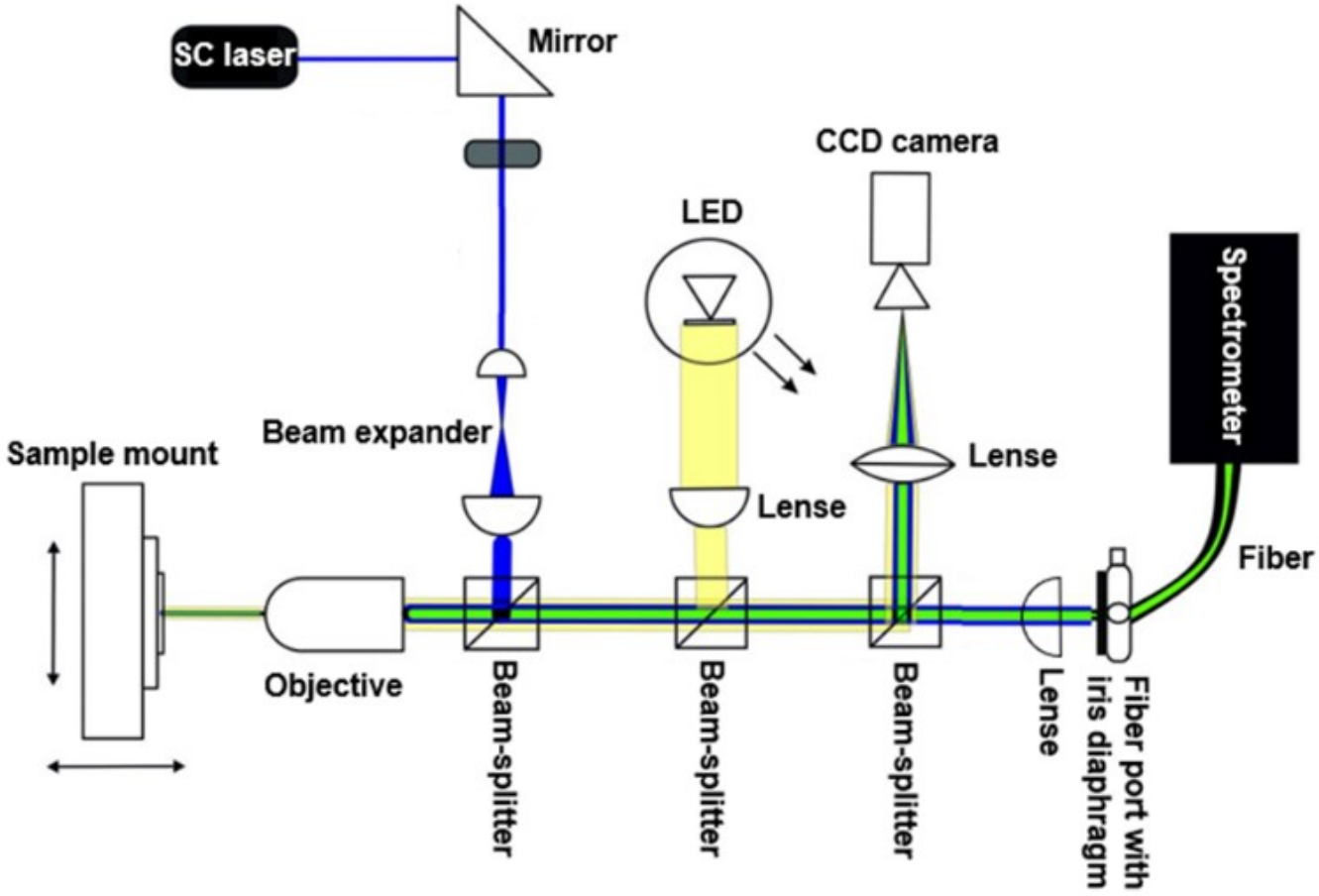

Figure S6. Schematic of the optical setup for transmittance measurements.

Modeling of the surface roughness impact on the waveguiding

To clearly demonstrate the impact of roughness on transmittance spectra in our simulations, we modified the top side of the waveguide with a randomly generated surface whose topography was set by a fixed correlation length (10 nm) and RMS values of 0, 15 and 40 nm. The calculated spectra (Figure S7) demonstrate a decrease in transmittance starting from 470 nm as the RMS increases due to arising scattering. However, in the near-IR, we obtain higher transmittance compared to the smooth waveguide. This slight enhancement is expected to result from an efficient cross-section enlargement due to roughness, whereby the cut-off wavelength associated with mode delocalization is red-shifted. At shorter wavelengths, RMS-induced scattering dominates over the enlargement of the waveguide cross-section.

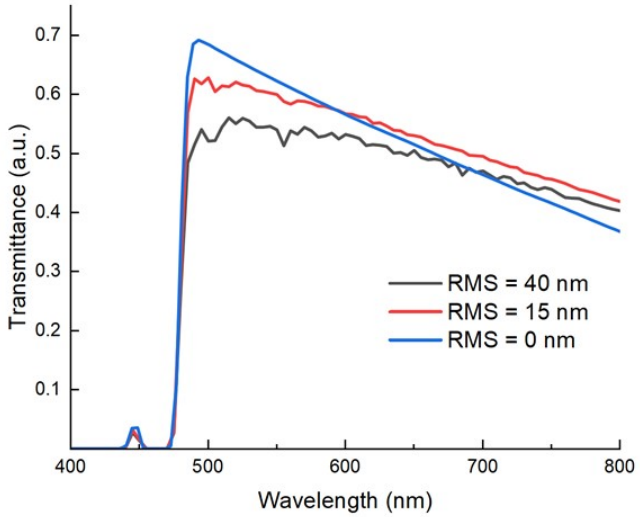

Figure S7. Transmittance spectra of a thin waveguide (70 x 1000 nm^2)

with different top side roughness

FIB-fabricated $GaInS_3$ waveguides

As an alternative to m-SPL, we fabricated strip waveguides using a xenon FIB milling procedure (Figure S8a). The SEM image in Figure S8b shows seven waveguides obtained from a 70 nm $GaInS_3$ flake with a length of 20 µm. At first glance, the waveguides appear structurally well fabricated. However, AFM profiles (Figure S8c) measured along the blue dashed line demonstrate a decrease in waveguide height for smaller cross-sections. Moreover, the enlarged profiles in Figures S8d–f show that the waveguides have a rounded rather than rectangular shape, so the actual cross-section is smaller than estimated. This effect occurs due to the Gaussian shape of the ion beam and its overlap while milling the waveguide from both side walls. The fabricated waveguides exhibited neither waveguiding nor Raman response (likely due to lattice damage from FIB ions).

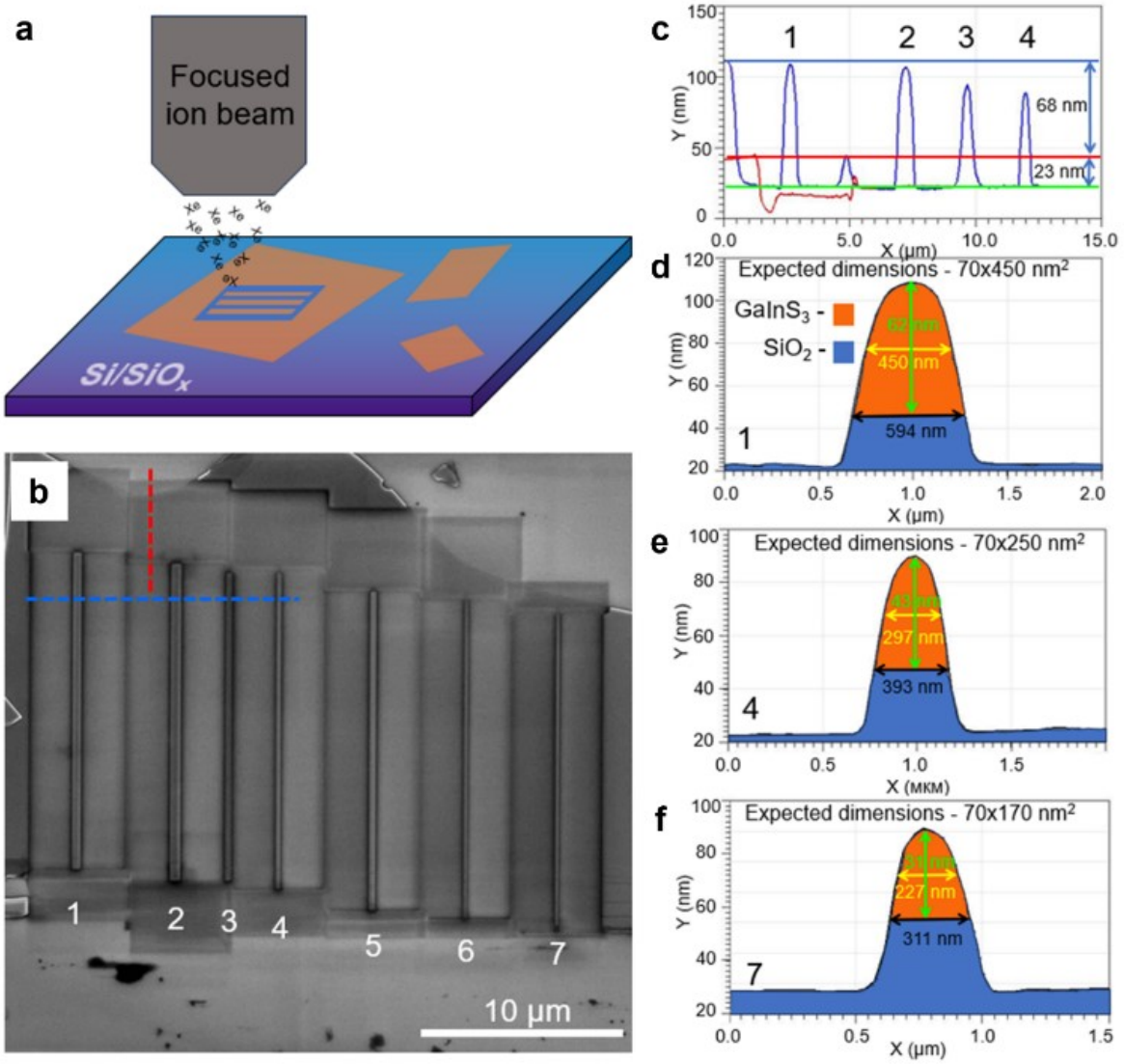

Figure S8. a) Schematic of the $GaInS_3$ strip waveguides milling by focused ion beam. b) SEM-mage of the fabricated waveguides. c) AFM-profiles along red and blue lines in b), red line indicates substrate level, green – substrate level with after milling, blue – height of the waveguides $GaInS_3$ fraction. d-f) enlarged profiles of the 1, 4, and 7 waveguides.

Supporting Information

Notes and references

1 A. N. Toksumakov *et al*., *NPJ 2D Mater Appl*, 2022, **6**, 85.
2 H. Yang *et al*., *arXiv*, 2024, *arXiv*:2405.04967.
3 A. Mazitov *et al*., *arXiv*, 2025, ш:2503.14118.
4 B. Mortazavi et al., *Physica E: Low Dimens. Syst. Nanostruct.*, 2017, **87**, 228–232.
5 T. Cui *et al*., *Matter*, 2022, **5**, 2975–2989.
6 B. Mortazavi, G. R. Berdiyorov, M. Makaremi and T. Rabczuk, *Extreme Mech Lett*, 2018, **20**, 65–72.